Design of a Top-Lit Up-Draft Micro-gasifier Biomass Cookstove by Thermodynamic Analysis and Fluent Modeling

Keily De La Hoz C. [*], Juan F. Pérez [*]‡, Edwin Lenin Chica Arrieta [**]

[*] Grupo de manejo eficiente de la energía- GIMEL, Departamento de Ingeniería Mecánica, Facultad de Ingeniería, Universidad de Antioquia; Calle 67, No. 53-108, Medellín, Colombia.

[**] Grupo de energía alternativa- GEA, Departamento de Ingeniería Mecánica, Facultad de Ingeniería, Universidad de Antioquia; Calle 67, No. 53-108, Medellín, Colombia.

(keilydelahozc@gmail.com, juanpb@udea.edu.co, edwin.chica@udea.edu.co)

‡ Corresponding author. Phone: (+57 4) 2198552. Fax: (+574) 2110507. e-mail: juanpb@udea.edu.co (J.F. Pérez).

Received: 04.04.2017 Accepted:25.07.2017

Abstract

In this work the complete thermo-mechanical design of a biomass top-lit up-draft (TLUD) cookstove is presented. A design methodology which is based on mass and energy balances, geometry relations among the main dimensions of the cookstove, and fluent modeling is proposed. Three models were designed, sized, and simulated through computational fluid dynamics (CFD) conducted in ANSYS Fluent 15.0.7. These designs allowed analyzing the effect of cookstove design, primary and secondary air inlets (diameter and air supply setup) required in the gasification and combustion processes, respectively. Simulations indicated that compressed air is not a suitable way to supply the air flow for gasification and combustion stages, due to the poor velocity distribution across the grate and secondary holes. Therefore, the final stove design will operate with axial fans to favor a good mixture between biomass and the air in the gasification stage, and between producer gas and the air in the combustion zone. Operation with axial fans, in the final cookstove design, allowed obtaining a low standard deviation of air velocity through the grate holes and through secondary air ring holes (±0.13 m/s, and ±0.45 m/s, respectively), which entails a better cookstove performance. This air supply system, also presented combustion air velocities through the secondary ring holes according to the ones reported in the literature (3.02 m/s), which is important for the suitable air and producer gas mixing.

Keywords: Biomass cookstove, micro-gasification, top-lit up-draft reactor (TLUD), design, thermodynamic analysis, CFD simulation.

1. Introduction

The food cooking is an elemental activity for all people; therefore, it has to be done using resources with high availability. Biomass is one of them, as a renewable energy source, it is used in developing countries for heating and cooking [1]. Hence, biomass constitutes approximately 40% of the world's population primary fuel [2], [3]. Traditional cookstoves based on biomass combustion are frequently used for this purpose, but they have low efficiency (<15%) generating social, environmental, and health impacts [3].

Indoor smoke from solid fuels affects a large portion of the world's population [4], it is estimated that 4.3 million of premature deaths per year around the world are caused due to indoor air pollution [5], [6], [7]. These deaths are attributed to harmful substances such as particulate matter, 21% of deaths due to respiratory infections, 35% of deaths due to chronic obstructive pulmonary diseases, and 3% of pulmonary deaths [8]; for this reason, many entities are concerned about harmful emissions produced by biomass fuel [9].

In Colombia about 1.6 million of families use firewood for cooking activities, 87.5% of them live in rural areas [10]. This activity is made without any emissions control, with inefficient combustion and limited ventilation, that can also produce acute lower respiratory infections, middle ear infections, nasopharynx cancer, perinatal disease and eye diseases, affecting mainly to women and children [11]. Moreover, it is known that 16% of outdoor pollution is caused by indoor pollution [12].

The environmental impacts are also increasing because of deforestation and the highest levels of pollutant emissions, aggravating global warming phenomenon [5], [6]. Biomass gasifier cookstoves represent an alternative to mitigate these

problems to a large extent [13], due to the high efficiency (>25%) and lower pollutants emissions (particulate matter and carbon monoxide).

For these reasons, improved biomass cookstoves have been studied from the energy and environmental point of view. Tryner et al. [14] characterized the emissions of a modular top-lit up-draft (TLUD) stove, varying the number and diameter of secondary air holes by different rings (removable rings). Gasification and combustion air were supplied by compressed air, controlling flows by rotameters, a similar work was presented by Vurunkumar [15]. Tryner et al. [14] designed the cookstove with two independent chambers, one for the primary air and the other one for the secondary air, unlike other designs from Reed et al. [16] where two concentric cylinders were used (reactor and secondary flow). TLUD cookstoves have also been designed with rectangular primary air chambers and gasification air supplied from fans [5], [17], [18]. These kind of stoves usually have a grate which holds the fuel stack [5], [19], [20], this grate is detachable in order to remove the ash after cooking. The material is another aspect for taking into account because it determines the weight, resistance to high temperatures and heat transfer, due to these facts cookstoves are built from stainless steel [19] and galvanized steel [20], althoungh there are others built from cast iron for prologing the life span [21]. Regarding heat losses, energy efficiency, and power output, some designers have considered insulating materials such as refractory brick, mud, wheat husk-mud mixture [21], layers of stainless steel, aluminum foil [18], and glass wool [19], among others. In Table 1 some important dimensions of TLUD cookstoves found in the literature are presented.

Usually, the gasification process in cookstoves is carried out in a top-lit up-draft reactor; this technology has been developed in order to reduce the fuel consumption, that can be achieved guaranteeing complete combustion, and at the same time, the soot production diminishes, improving the air quality of many families who use this fuel to supply their daily energy demand [22]. The gasification process is already known for several advantages on the environmental level [23], and adapting it to a small scale (micro-gasification) in improved cookstoves represents portability, saving of fuelwood consumption, and reduction of diseases [22], [24]. There are also some disadvantages related to forced draft cookstoves, so, they are more expensive to build and operate in comparison with natural draft cookstoves. Therefore, the aim of this work is to present a detailed design methodology of a biomass micro-gasification improved cookstove, which is scarce in the literature consulted and in the country. This work also contributes to strengthen the improved cookstoves program guidelines promoted by the Colombian Ministry of Environment [25], and other international programs promoted by The Global Alliance for Clean cookstoves-GACC [26], Africa Clean Cooking Energy Solutions-ACCES [27], and Energising Development- EnDev [28].

2. Design Methodology

In Top-lit Up-draft cookstoves, biomass within the reactor is lit from the top of the bed; during the gasification process there is a pyrolytic front formation which progresses downwards leaving char at the top of the raw biomass (fuelstack). Oxidation reactions cause a depletion of the oxygen, and heat generated above favors the volatile matter production within an inert atmosphere. In TLUD cookstoves, primary air is supplied from the bottom of the reactor and it is necessary for the gasification process. A combustion air (secondary air) which mixes with the producer gas, and reacts for generating the power required during the cooking process. These stages are pointed out in Fig. 1.

To design a biomass cookstove, the main parameters required are the thermal power and fuel type, considering that cookstoves dimensions depend principally on them.The aim of this work is to design a biomass cookstove between 0.2-10 kW to build an experimental setup. The energy performance assessment of the cookstove requires a modular gasifier stove to interchange some important dimensions like diameter of the secondary air inlets in the ring [14]. It is also necessary to visualise the primary and secondary flows that are going into the gasification and combustion zones [15], [16]. The power of cookstoves found in the literature (see Table 1) varies from 2 to 3.5 kW, the power is determined by the diameter of the reactor, since there is a proportional relationship between the stove diameter and its power. On the other hand, the reactor height determines the biomass consumption time and syngas quantity. These parameters (reactor diameter and height) are extremely important because in the experimental setup, it is necessary to place the cookstove over a digital balance to measure the mass changes during the process [14], [15], [19] as can be seen in the experimental setup shown in Fig. 2.

2.1 Cookstoves dimensions

The power (Q) can be expressed in function of the low heating value (LHV) and fuel consumption rate ($\dot{m}_{bms}$). As design criterion, the cookstove efficiency (E) was taken as 25% according to Issue and Saloop [30]. Equation (1), is used to determine the biomass consumption rate.

$$\dot{m}_{bms} = \frac{Q}{E * LHV} \quad (1)$$

By means of a relation between the biomass consumption rate ($\dot{m}_{bms}$), and specific biomass consumption rate ($\dot{m}'_{bms}$), the reactor diameter (D) is calculated from equation (2). The specific biomass consumption rate of wood pellet #2 was studied and presented by Porteiro et al. [31] (see Table 2). This parameter was calculated considering the flame front velocity and the biomass bulk density. The specific biomass combustion rate is taken to be 0.045 kg/m^2/s [31], as design criterion. This value is considered due to the fact that lower air flows favor the biomass gasification process (high gasification efficiency).

$$D = \sqrt{\frac{4 * \dot{m}_{bms}}{pi * \dot{m}'_{bms}}} \quad (2)$$

Table 1. Main dimensions of cookstoves reported in the literature.

Cookstove	Reactor height [mm]	Reactor diameter (D) [mm]	External diameter (d) [mm]	Secondary holes (number x diameter)	Ref.
1	600	206	222	3 x (20*190)mm	[29]
2	130	100	-	18 x Ø5mm	[19]
3	719	206	-	Pipes -12 x 290 mm - Ø12 mm	[17]
4	300	207	253	32 x Ø15 mm	[21]
5	300	203	303	24 x Ø15 mm	[21]
6	300	226	320	20 x Ø15 mm	[21]
7	220	166	220	-	[20]
8	135	130	150	30 x Ø4 mm	[18]
9	210	100	-	18 x Ø50 mm	[18]
10	180	145	-	14 x Ø4 mm	[18]

The bed height (h) depends on the set time for the total biomass consumption inside the reactor, the biomass consumption per unit area ($\dot{m}'_{bms}$), and the biomass bulk density (den_{bms}) as is expressed in the equation (3).

$$h = \frac{\dot{m}'_{bms} * t}{den_{bms}} \quad (3)$$

2.2 Primary air flow for biomass gasification

During the thermochemical conversion process of biomass, it is necessary to supply a gasifying agent that can be air, steam water, carbon dioxide, and oxygen. TLUD cookstoves use atmospheric air to favor the conditions for the incomplete oxidation reactions (gasification); this air is supplied from the bottom of the reactor and is also known as primary air flow. The primary air aeration factor is the relation between real air-fuel and stoichiometric air-fuel ratios (see equation 4). It is estimated that during the gasification process around 20% - 40% from the stoichiometric air is used, in order to reach a partial oxidation [32]. In this work, as design criterion a primary air aeration factor of 0.4 ($w = 0.4$) is considered, see equation (4).

$$w = \frac{(A/F)real}{(A/F)stq} = 0.4 \quad (4)$$

By means of the biomass substitution formula $CH_{1.49}O_{0.55}$ in a stoichiometric reaction with air, the air-fuel stoichiometric ratio is found, as expressed in equation (6).

$$CH_{1.49}O_{0.55} + a(O_2 + 3.76N_2) \rightarrow xCO_2 + eH_2O + zN_2 \quad (5)$$

$$(A/F)stq = \frac{4.76 * a * M_a}{1 * M_{bms}} \quad (6)$$

Afterwards, primary air volumetric flow is found, considering 40% of stoichiometric air, as can be seen in equation (7).

$$\dot{V}_a = \frac{0.4 * (A/F)stq * \dot{m}_{bms}}{den_a} \quad (7)$$

2.3 Secondary air flow for the producer gas combustion

The secondary air is supplied to oxidize the bio-syngas produced by the biomass gasification process; this reaction (combustion) releases the thermal energy to cook the meals. The producer gas composition assessment starts from the moles of calculated air in the stoichiometric reaction (a) in the equation (5), and the complete balance with an aeration factor of $w = 0.4$. The global gasification reaction is shown in equation (8) [33].

$$CH_{1.49}O_{0.55} + aw(O_2 + 3.76N_2) \rightarrow x'CO_2 + yCH_4 + z'N_2 + bH_2 + cCO + e'H_2O \quad (8)$$

There are 6 unknown variables and only 4 equations, thereby, it is necessary to turn on dissociation reactions for solving the equations system. The first reaction is due to methane formation, which comes from hydrogen reduction (see equation 9) [32], [34].

$$C + 2H_2 \rightarrow CH_4 \quad (9)$$

The equilibrium constant for the last reaction is shown in equation (10).

$$K_1 = \frac{y}{b^2}\left(\frac{P_{atm}}{x' + y + z' + b + c + e'}\right)^2 \quad (10)$$

The second dissociation reaction is the water-gas shift reaction, which describes the equilibrium between CO and H_2 with water, see equation (11).

$$CO + H_2O \rightarrow CO_2 + H_2 \quad (11)$$

The equilibrium constant for the water-gas shift reaction is presented below in the equation (12).

$$K_2 = \frac{x' b}{c\, e'} \quad (12)$$

Table 2. Properties of biomass fuel, Wood pellet #2. Adapted from [31]

Biomass properties	
Moisture [%]	7.7
Volatile matter [%]	67.9
Fixed carbon [%]	22.6
Ash [%]	1.8
LHV [kJ/kg]	18300
Particle density [kg/m^3]	1240
Bulk Density [kg/m^3]	680
Equivalent radius [mm]	4.4
Sphericity [-]	0.84
Porosity [-]	0.45
Substitution formula [dry ash free]	$CH_{1.49}O_{0.55}$

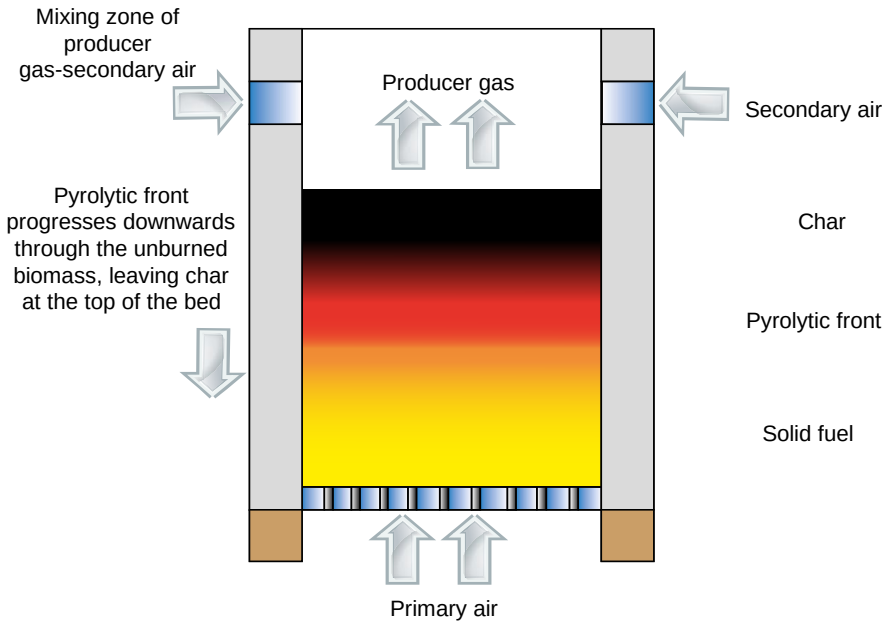

Fig. 1. Micro-gasification process in TLUD cookstoves.

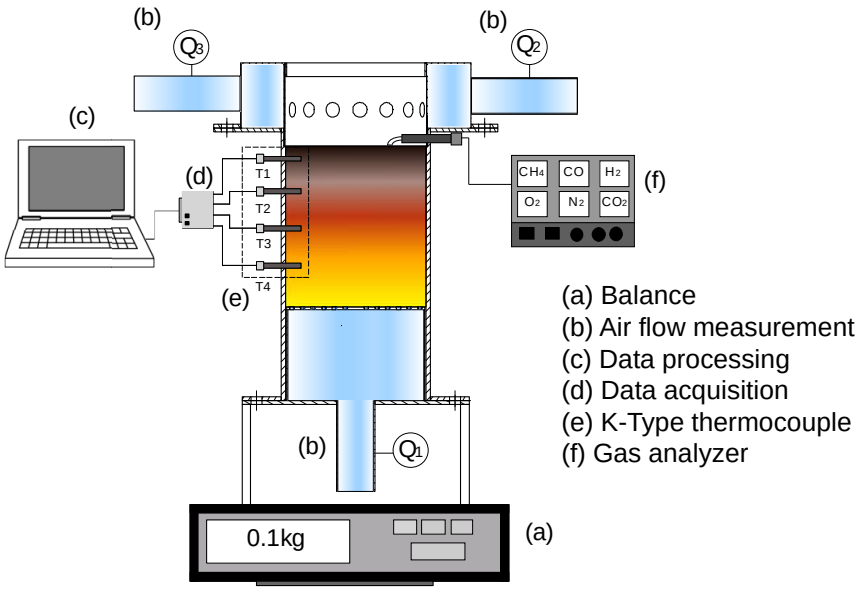

Fig. 2. Experimental setup with acquisition and display systems

The equations (10) and (12) complete the mathematical balance to solve the non linear equation system, it allows estimating the moles quantity of all the gaseous products. The equilibrium constants were taken at 1200 K [35].

In the combustion phase, the most important elements are (C_xH_y), carbon monoxide (CO) and hydrogen (H_2), because these gaseous fuels react with the secondary air that is fed through the secondary holes. Afterwards, the mole fraction of each product was calculated (see equation 13) to describe the producer gas oxidation reaction with air.

$$Y_i = \frac{n_i}{n_T} \tag{13}$$

The stoichiometric reaction of the gaseous fuels with air is expressed by the equation (14).

$$Y_{CH_4}CH_4 + Y_{CO}CO + Y_{H_2}H_2 + a'(O_2 + 3.76N_2) \rightarrow x''CO_2 + e''H_2O + z''N_2 \tag{14}$$

Considering only the combustible gases, the new stoichiometric air-gas ratio can be expressed based on the combustion air mass flow. See equation (15).

$$(A/F)stq,g = \frac{\dot{m}_{air,c}}{\dot{m}_g} \tag{15}$$

According to the variables from equation (15), the producer gas mass flow ($\dot{m}_g$, kg/s) must be known; this parameter can be estimated through the primary air volumetric flow, making the following considerations [36]: 1) the mass flow of N_2 present in the primary air, can be assimilated to the mass flow of N_2 present in the syngas, and 2) the nitrogen mass flow from biomass, derived from the ultimate composition, is smaller compared with the N_2 present in the air. Thus, the mass balance of nitrogen in the process is presented in equation (16).

$$\dot{m}_{N_{2,bms}} + \dot{m}_{N_{2,air}} = \dot{m}_{N_{2,g}} \tag{16}$$

According to the consideration $\dot{m}_{N_{2,bms}} \ll \dot{m}_{N_{2,air}}$, the producer gas volumetric flow can be determined from the nitrogen mass balance as shown below in equation (17).

$$\dot{V}_{g,norm} = \frac{den_{N_{2,std}} * \dot{V}_{air,std} * Y_{N_{2,air}}}{den_{N_{2,norm}} * Y_{N_{2,g}}} \tag{17}$$

The producer gas mass flow is estimated with its density under normal conditions, according to the mixture gas law [37].

$$\dot{m}_g = den_{g,norm} * \dot{V}_{g,norm} \tag{18}$$

2.4 Secondary air inlets sizing

For sizing the secondary air holes of the ring (at the producer gas combustion stage), the diameter (d_1) and separation (b) among them were set as design criterion; therefore, the number of holes can be found as follows, see equation (19).

$$N = \frac{P}{(d_1 + b)} \tag{19}$$

Diameter and separation values that were taken as a design criterion are based on the air flow velocity magnitude through the holes, since these variables are dependent, for this reason, it was taken as reference secondary air velocities reported in the literature for TLUD cookstoves, in order to keep this parameter according to the ones studied in previous works [14]. The velocity through the secondary air holes is calculated from equation (20).

$$v = \frac{4 * \dot{V}_{ac}}{N * pi * {d_1}^2} \tag{20}$$

3. Sizing of the TLUD Micro-gasifier Cookstove

The dimensions described in sections 2.1 and 2.4 were calculated taking into account the main TLUD cookstoves dimensions showed in Fig. 3 for each one of the three design configurations proposed in this work (M1, M2, and M3)

3.1 Reactor diameter and secondary air chamber diameter

The reactor diameter was calculated by means of equation (2), considering as design criterion a power range between 0.2-10 kW for the TLUD cookstove. In the Table 3, the effect of power on the reactor diameter is presented.
Once the reactor diameter has been found, TLUD cookstoves dimensions reported in the literature (see Table 1) were taken to determine the external diameter (secondary air chamber diameter), by setting out a geometrical ratio between reactor diameter: external diameter (D:d ratio) as shown in equation (21).

$$\frac{D}{d} = 0.6 \tag{21}$$

Reactor diameter and external diameter dimensions are very similar to the ones found in the literature (see Table 1). The power of the stoves found in the literature varies between 3.5-6.5 kW. From calculated parameters in Table 3, it can be seen the biomass consumption increases 0.79 kg/kW-h if cookstove power increases.

3.2. Bed Height

The equation (3) shows that bed height depends on biomass properties such as bulk density, specific biomass consumption rate and set time for the fuel consumption in the batch, therefore, this height is evaluated at different times (suggesting different cooking times). For the cookstove designs, it was selected a bed height between 3600-5400 s for configuration M1 (0.28 m), and between 2400-3000 s for configuration M2 and M3 (0.18 m) as can be seen in Table 4.

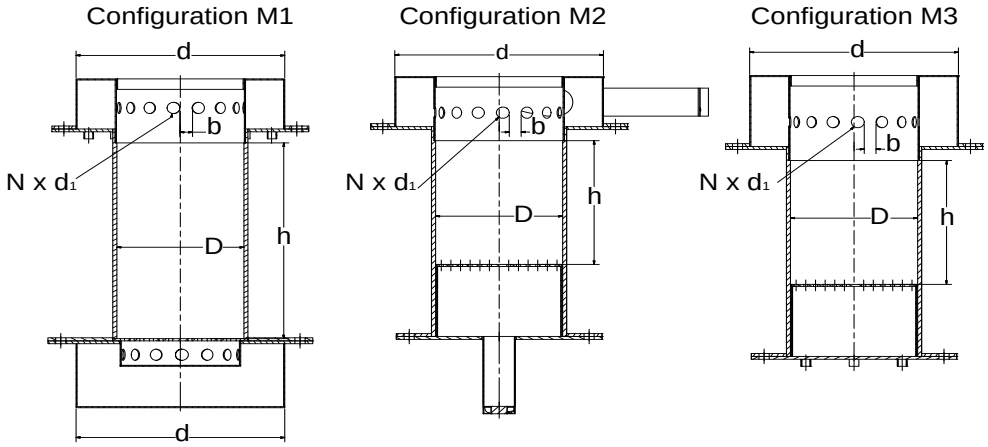

Fig. 3. Main dimensions of proposed TLUD cookstoves

Table 3. Reactor diameter and external diameter in function of cookstove power.

Stove	Power $Q\ [kW]$	Biomass consumption $\dot{m}_{bms}\ [kg\ s^{-1}]$	Reactor diameter $D\ [m]$	External diameter $d\ [m]$
1	3.5	0.000765	0.147	0.245
2	4.5	0.000984	0.166	0.278
3	5.5	0.001202	0.184	0.307
4	6.5	0.001421	0.200	0.334
5	7.5	0.001639	0.215	0.359
6	8.5	0.001858	0.229	0.382
7	9.5	0.002076	0.242	0.404
8	10	0.002186	0.247	0.414

These cooking times were selected considering technical parameters of an experimental setup such as weight and size.

Table 4. Bed height.

Cooking time (s)	Bed Height $h\ [m]$
1800	0.1191
2400	0.1588
3000	0.1985
3600	0.2382
5400	0.3574

3.3 Primary and secondary air flows

Considering the substitution formula of biomass $CH_{1.49}O_{0.55}$, chemical reactions were calculated as described in sections 2.2 and 2.3. In this way, primary and secondary air flows were found according to the cookstove power, these values are presented in Table 5.

The relation between primary and secondary air flows is recommended to have a 1:3 ratio to carry out experimental tests in cookstoves. In this way, the cookstove efficiency will be better [14], [16], [38]. Thus, the experimental flow with a primary: secondary ratio of 1:3 is also calculated in Table 5.

Fig. 4 shows the gasification air flow (primary, $\dot{V}_a$), combustion air flow (secondary, $\dot{V}_{ac}$), biomass consumption $(\dot{m}_{bms})$, and reactor diameter (D) in function of cookstove power. As it can be observed, if the power increases all geometrical and operational parameters increase too, this is due to the mass and energy conservation [39].

3.3.1 Secondary air holes diameters

The values taken as design parameters for secondary holes diameter, and separation among them, are shown in Table 6. According to the equation (19), the number of holes for the air passage to the combustion zone is defined. It is also calculated the theoretical velocity through each one using the equation (20).

3.4 Sizing with commercial materials

Diameters previously calculated in sections 3.1 and 3.3.1 are theoretical; therefore, it is important to design with commercial dimensions and available commercial materials in order to reduce costs. In this section, diameters, velocities, and power are re-calculated, taking into account commercial catalogues [40].

3.4.1 Reactor diameter, and secondary air chamber diameter

The reactor diameter is calculated from equation (2), this theoretical reactor diameter needs to be approximated to a commercial steel cylinder; thereby, other parameters such as power, biomass consumption, and external diameter (see equations 1, 2, and 21, respectively) are re-calculated. The

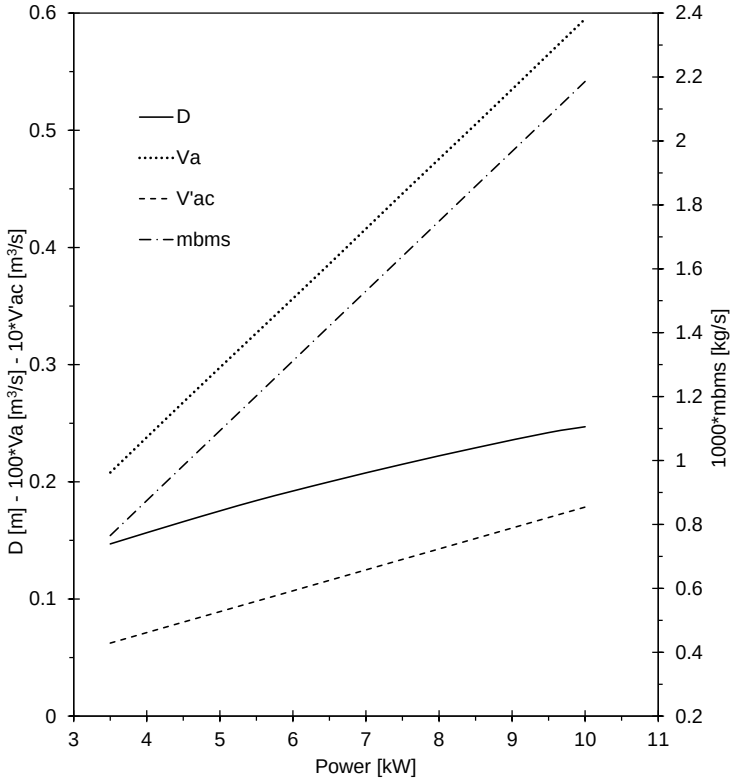

Fig. 4. Air flows, biomass consumption, and diameter variation according to the cookstove power.

new values for these diameters are shown in Table 7, where thickness was also taken into account by referencing a commercial catalogue [40]. In Fig. 5 the dimensions of the commercial reactor diameters specified in Table 7 are shown.

3.4.2 Primary and secondary flow

The primary and secondary air flows are re-calculated because they depend on the cookstove power and biomass consumption, in Table 8 the new parameter values are shown.

Table 5. Primary and secondary air flows.

Stove	Power $Q\ [kW]$	Gasification air flow $\dot{V}_a\ [m^3\,s^{-1}]$	Combustion air flow $\dot{V}_{ac}\ [m^3\,s^{-1}]$	Combustion air flow (1:3 ratio) $\dot{V}'_{ac}\ [m^3\,s^{-1}]$
1	3.5	0.00208	0.01118	0.00624
2	4.5	0.00268	0.01437	0.00803
3	5.5	0.00327	0.01756	0.00981
4	6.5	0.00386	0.02076	0.01159
5	7.5	0.00446	0.02395	0.01338
6	8.5	0.00505	0.02714	0.01516
7	9.5	0.00565	0.03034	0.01695
8	10	0.00595	0.03193	0.01784

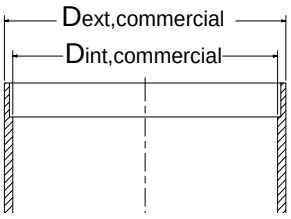

Fig. 5. Internal and external commercial diameters of the reactor.

3.4.3 Secondary air holes diameter

Due to the commercial size of the internal reactor diameter, the secondary air holes need to be corrected. This correction looks for ensuring the design adaptation to commercial materials and to develop more simple construction process by means of standardized parts of the cookstove. These secondary air characteristics are shown in Table 9.

3.5 Design models

To analyze the velocity profiles inside the stove, three designs are proposed (M1, M2, and M3), which were selected taking into account previous sensibility analyses of simulations carried out for several cookstoves designs. These cookstoves were modelled for a set power of 4.05 kW, this power was selected considering the middle of the design range 0.2-10 kW, moreover the fixed power is a favorable

scale for household cooking tasks [30]. Therefore, air supply in the primary and secondary zones were simulated.

Configuration M1: This design can be observed in Fig. 6. It has a chamber in the bottom where the primary compressed air is supplied through four air inlets (zone 1), in this place, the air is distributed through the holes of the ring before flowing across the grate to the bed where the gasification process happens (zone 2). The secondary air zone also has a chamber, in this stage the combustion air is also supplied by a compressor system and distributed through 16 holes to favor the mixing with the producer gas (zone 3)

Configuration M2: This second model is shown in Fig. 7. In this design, the grate used for the air passage is inside and concentric to the reactor (zone 1), in this way, the primary air passes directly to the bed zone where reacts with the biomass (zone 2). On the other hand, the secondary air is supplied by two fans that are coupled to pipes. These pipes are tangential to the secondary air chamber.

Configuration M3: This configuration is pointed out in Fig. 8. It has two ways of supplying air, compressed air in the gasification stage, composed by four inlets distributed every 90º, and for the secondary air supply, there is a fan coupled to a pipe which is tangential to the secondary air chamber. The grate where primary air flows to the fuel stack is inside the reactor and concentric to it.

Table 6. Secondary air holes dimensions.

Stove	Power $Q\ [kW]$	Perimeter $P\ [m]$	Holes diameter $d_1\ [m]$	Separation $b\ [m]$	Number of holes N	Air velocity through each hole $v\ [m\ s^{-1}]$
1	3.5	0.4622	0.016	0.014	15	3.61
2	4.5	0.5241	0.016	0.014	17	4.09
3	5.5	0.5794	0.016	0.014	19	4.52
4	6.5	0.6299	0.016	0.014	21	4.92
5	7.5	0.6766	0.016	0.014	22	5.28
6	8.5	0.7203	0.016	0.014	24	5.62
7	9.5	0.7615	0.016	0.014	25	5.94
8	10	0.7813	0.016	0.014	26	6.10

Table 7. Commercial diameters.

Power $Q\ [kW]$	Biomass consumption $\dot{m}_{bms}\ [kg\ s^{-1}]$	Reactor diameter (theoretical) $D\ [m]$	External commercial reactor diameter $D_{ext,commercial}\ [m]$	Internal commercial reactor diameter $D_{int,commercial}\ [m]$	External commercial diameter $d\ [m]$
3.49	0.000764	0.147	0.153	0.147	0.245
4.05	0.000886	0.166	0.1683	0.1583	0.260
6.21	0.001358	0.184	0.204	0.196	0.326
6.47	0.001414	0.200	0.206	0.200	0.333
9.79	0.002139	0.242	0.254	0.246	0.410

Table 8. Primary and secondary flows according to the power.

Power $Q\ [kW]$	Internal commercial reactor diameter $D_{int,commercial}\ [m]$	Gasification air flow $\dot{V}_a\ [m^3\ s^{-1}]$	Combustion air flow $\dot{V}_{ac}\ [m^3\ s^{-1}]$	Combustion air flow (1:3 ratio) $\dot{V}'_{ac}\ [m^3\ s^{-1}]$
3.49	0.147	0.00208	0.01116	0.00623
4.05	0.1583	0.00241	0.01294	0.00723
6.21	0.196	0.00369	0.01984	0.01108
6.47	0.200	0.00385	0.02065	0.01154
9.79	0.246	0.00582	0.03125	0.01745

Table 9. Secondary air holes characteristics.

Power $Q\ [kW]$	Secondary holes ring diameter	Perimeter $P\ [m]$	Holes diameter $d_1\ [m]$	Separation $b\ [m]$	Number of holes N	Air velocity through each hole $v\ [m\ s^{-1}]$
3.49	0.149	0.4681	0.016	0.015	15	3.68
4.05	0.1623	0.5099	0.016	0.015	16	3.86
6.21	0.200	0.6283	0.016	0.015	20	4.87
6.47	0.203	0.6377	0.016	0.015	21	5.02
9.79	0.250	0.7854	0.016	0.015	25	6.13

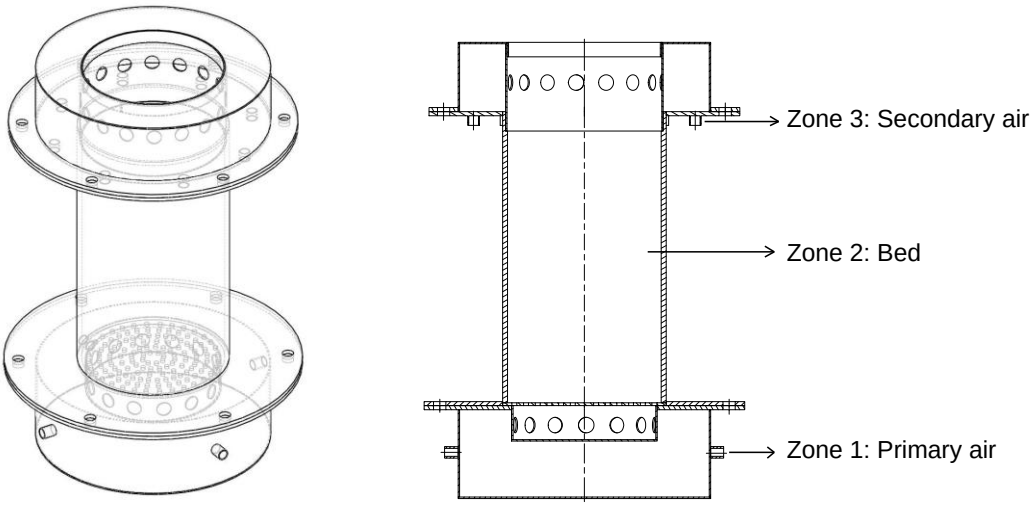

Fig. 6. Configuration M1.

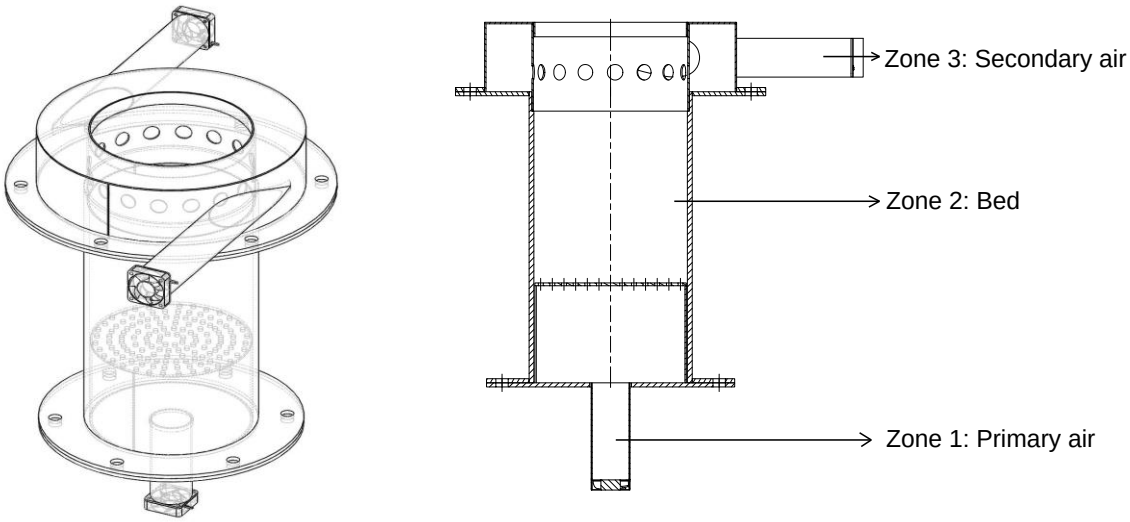

Fig. 7. Configuration M2.

4. Numerical Results and Analysis

The air distribution inside the three designs is analyzed by means of a model developed in the ANSYS Fluent 15.0.7 software [41]. The model is used to simulate fluid-dynamic parameters for analyzing the velocity fields in two zones of the TLUD cookstove; these zones are: 1) the grate holes where the primary air flows to the bed (zone 1), and 2) the secondary air ring holes where the secondary air flows to the producer gas combustion (zone 3). The biomass was loaded considering a porous media (solid biomass particles), where the physical properties of biomass such as particle density, packing factor (PF), and porosity thresholds were included [41].

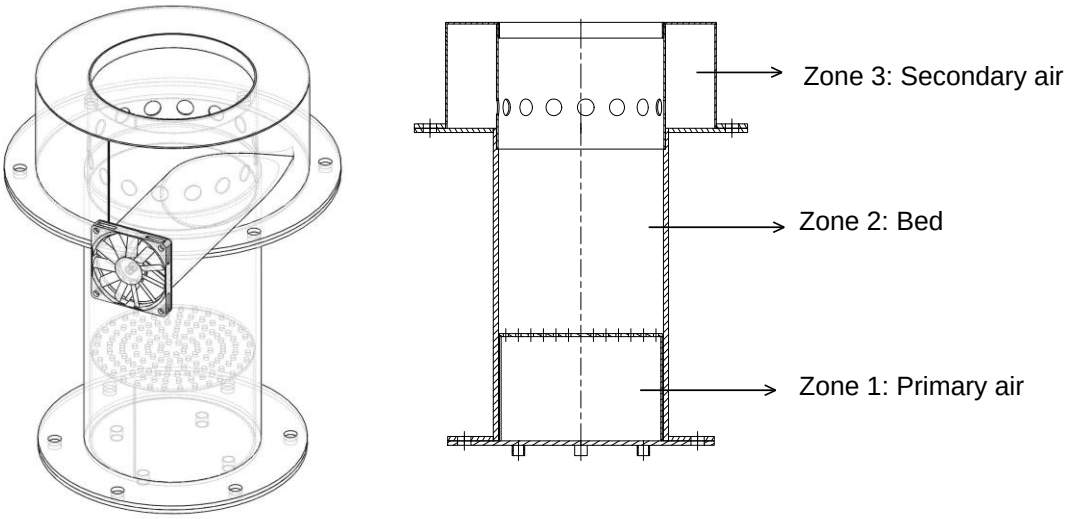

Fig. 8. Configuration M3.

These properties are loaded into the bed zone for restricting the primary air flow passage throughout it. Using this model brings some advantages, because if physical properties are taken into account in the reactor, simulations results can be near the experimental ones, so, the air distribution and cookstove performance can be predicted.

4.1 Zone 1: Velocity profiles of primary air

M1 configuration: Fig. 9 (a), shows the primary air inlet in the M1 configuration. Air supply was simulated as compressed air [14] as described before (see section 3.5). The inlet holes of gasification air are placed laterally in the zone 1; these holes have a diameter of 11 mm. The air velocity in each compressed air inlet reaches magnitudes up to 8 m/s. This velocity prevents a homogeneous distribution of the fluid across the grate, where a radial velocity increase from inner to external holes happens. The average velocity of air through the grate holes for this configuration is 1.01±0.26 m/s, as can be seen in Fig. 10.

M2 configuration: In Fig. 9 (b) the velocity field in the M2 configuration is presented. The air supply consists of a piping system of 40 mm diameter, concentric to the reactor and directly connected to an axial fan (see Fig. 7). The maximum velocity reached by the air in this primary inlet has a magnitude of 3.34 m/s due to the bigger injection area. This lower primary velocity with regard to M1 configuration allows a better distribution of the fluid across the grate holes. The homogeneous distribution of primary air velocity is supported by the lowest standard deviation. The average velocity in the center of the holes from the grate is 1.03±0.13 m/s (see Fig. 10).

M3 configuration: The velocity field of this configuration can be seen in Fig. 9 (c), the air is supplied by compressed air through 4 holes of 11 mm in diameter. The velocity in each one of the inlets reached magnitudes up to 8 m/s, there is also a radial velocity increasing of 0.63 m/s from the inner to the external grate holes. In this configuration, in the Fig. 10 is shown that the air passes through the grate with an average velocity of 1.0±0.25 m/s.

4.2 Zone 3: Velocity profiles of secondary air

For the secondary air analysis, a straight line (the black line) was drawn in the ANSYS Fluent 15.0.7 software for each configuration (M1, M2, and M3). This line passes through the secondary air inlet and goes through two holes (opposed between them) of the secondary air ring as can be seen in Fig. 11, in this way, the software allows plotting the air velocity versus position throughout the line (see Fig. 12). The standard deviation of velocity through the ring holes is also calculated, because it allows knowing which configuration presents the most uniform velocity in this zone, what is suitable for a better mixture between air and producer gas.

M1 configuration: The secondary air supply in this configuration has eight holes with 11 mm in diameter, which are placed on the lowest disk of the secondary air chamber, which is located in the zone 3, as can be seen in Fig. 11 (a). Each one of the compressed air inlets reaches velocities of 8.5 m/s, as can be seen in the velocity peaks of the Fig. 12. In this configuration, the secondary air holes around the ring operate with an average air velocity of 2.52±0.053 m/s (see Fig. 13). This is the lowest standard deviation due to the high number of air flow inlets distributed around the secondary air chamber. However, it makes that the manufacture and compressed air supply, become more complex and expensive processes, for this reason, this configuration is not feasible. Moreover, there is a backflow in the zone 3 which is evident with 0 m/s velocities that cause unnecessary energy losses (see Fig. 11 a)

M2 configuration: This configuration can be observed in Fig. 11 (b), it has two tangential inlet pipes (40 mm diameter), where the air is supplied by axial fans coupled to the piping system. Velocities in these tangential inlets are up to 3.34 m/s due to the pipe area. The secondary air (for the combustion process) through the ring holes has an average velocity of 2.55±0.45 m/s (see Fig. 13). This velocity is within the ranges reported in the literature (up to 5 m/s)

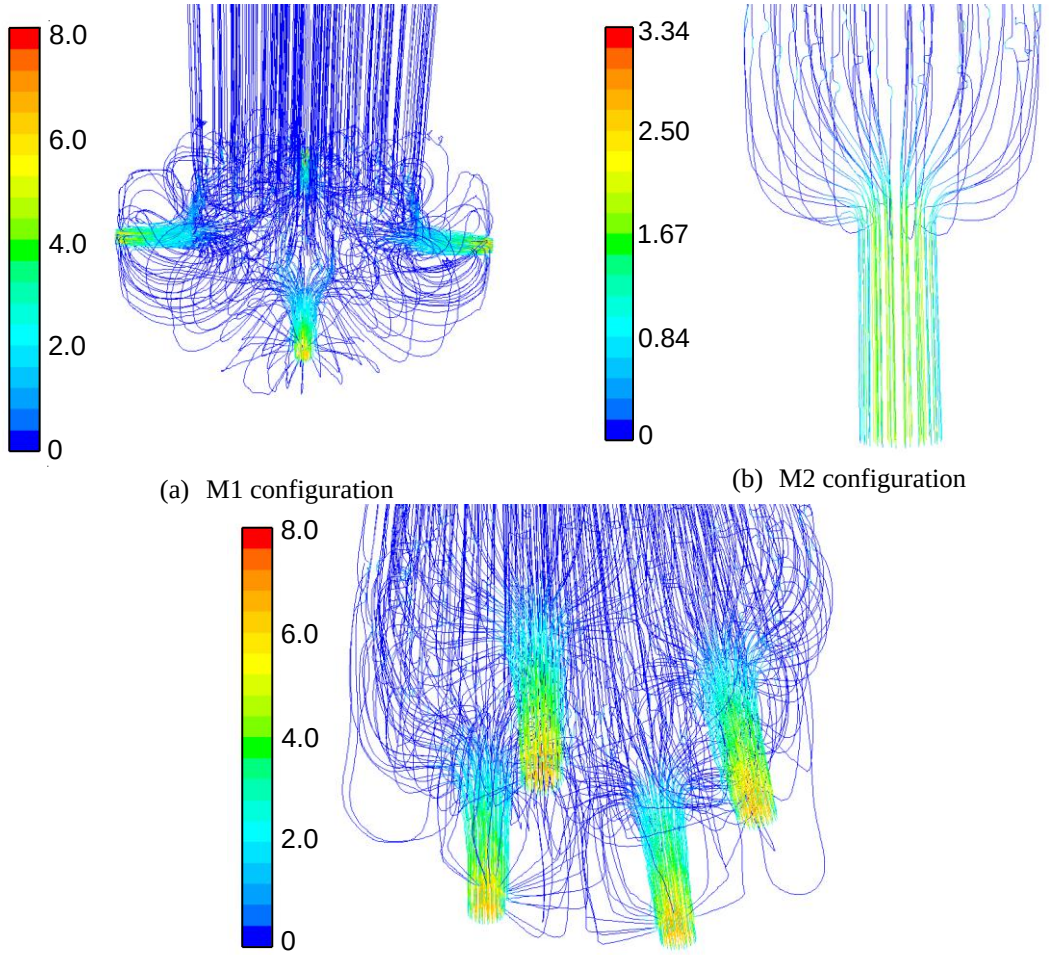

(a) M1 configuration (b) M2 configuration

(c) M3 configuration

Fig. 9. Velocity pathlines of the primary air inlet for the different designs in zone 1. Velocity in m/s.

studied by Tryner et al. [14]. The velocity through the holes that the line showed in Fig. 11 touches, has a magnitude of 3.02 m/s as can be seen in the velocity distribution of Fig. 12.

M3 configuration: The M3 configuration can be seen in Fig. 11 (c), it has only one tangential air inlet tube with 80 mm diameter, the air is supplied from an axial fan connected to the piping where the secondary flow for the producer gas

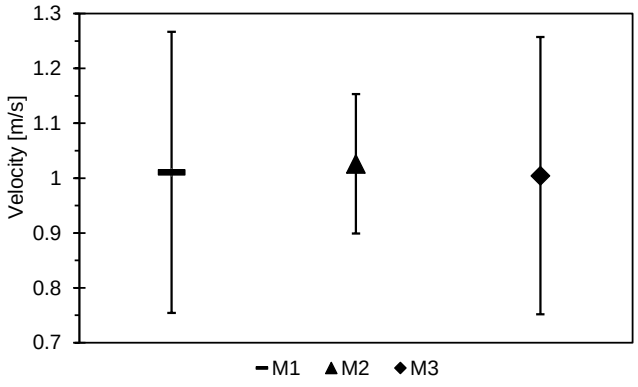

Fig. 10. Primary air velocity across the grate holes and standard deviation.

combustion process is delivered. The air velocity through the line drawn in Fig. 11 (c) shows that the holes closest to the main air inlet has a velocity of 3.49 m/s and the furthest (opposed to it) reach rates of 1.99 m/s (see Fig. 12). This happens because air takes as preferential paths the holes closest to the main air inlet, and the remaining secondary air flow is distributed through the furthest holes. This leads to poor uniform mixing between combustion air and producer gas. The average velocity of air through the ring holes is 2.60±0.60 m/s.

4.3 Design of the TLUD micro-gasifier biomass cookstove

Analyzing the velocity distribution and simulation results (mainly the standard deviation) in the primary and secondary air, the M2 configuration has the better velocity field due to the suitable distribution across the grate holes, which is important for ensuring stability in the reaction front during the biomass gasification process [42]. Regarding the secondary air (zone 3), the better configuration is M1 due to the uniform velocity field through the secondary ring holes, but from a manufacturing point of view, it is not an appropriate design because of high setup costs (compressed air accessories). This means that the M2 configuration is the

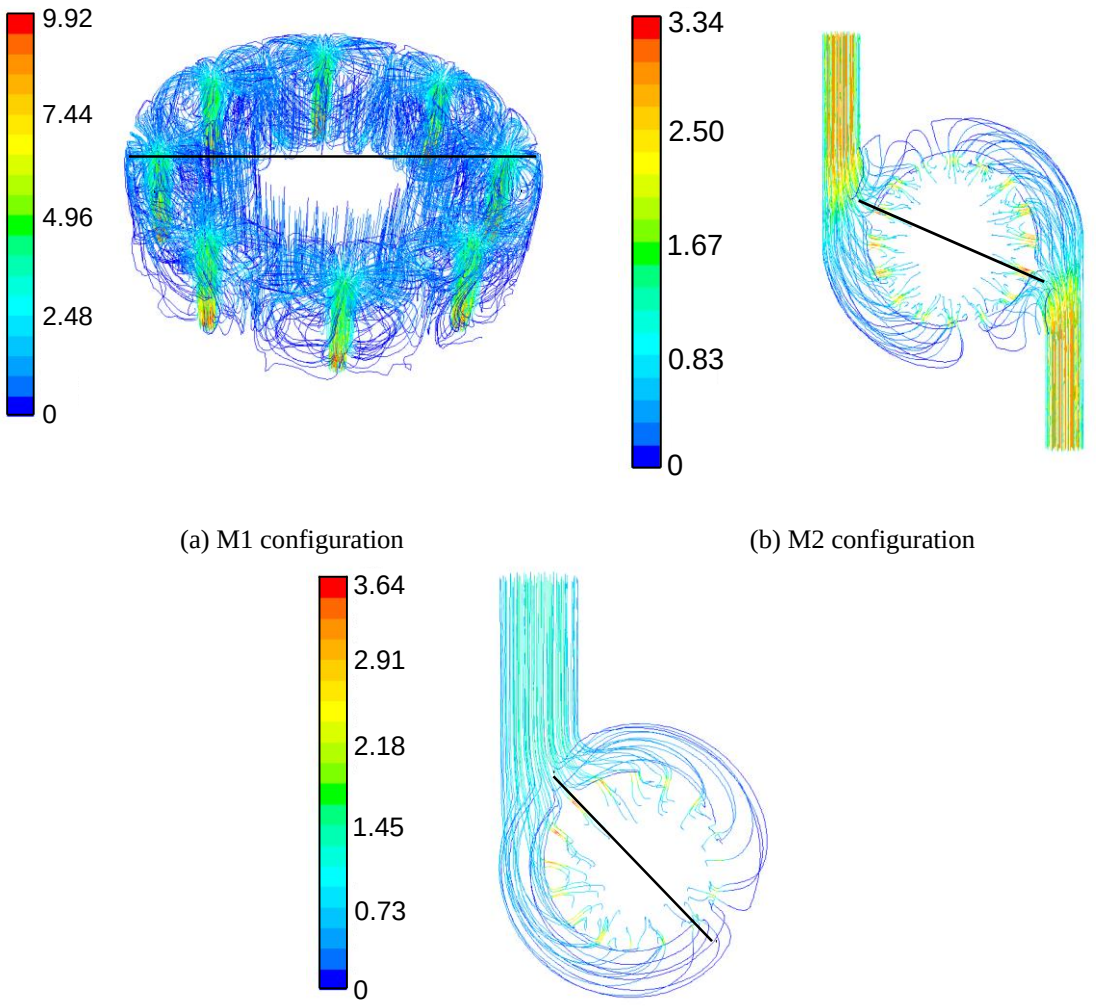

(a) M1 configuration (b) M2 configuration

(c) M3 configuration

Fig. 11. Velocity pathlines of the secondary air inlet for the different designs in zone 3. Velocity in m/s

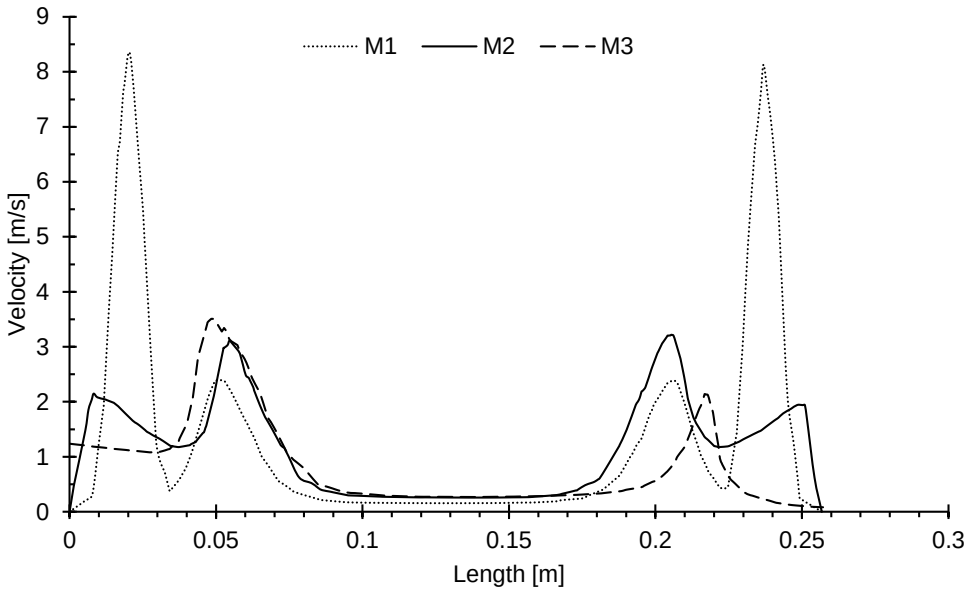

Fig. 12. Velocity vs. Length, through the line in the secondary air zone.

well-adjusted cookstove design (see Fig. 14). Moreover, forced draft cookstoves prototypes operate with pc coolers [6], [15], [16]; for this reason, these kind of accessories will allow making experimental tests using a prototype that has been already used for TLUD cookstoves (product design).

5. Conclusions

Compressed air to supply the primary and secondary air allows a better control of flows due to the easy use of rotameters; these instruments have already been used for applications in cookstoves, but the poor distribution observed across the grate velocity field with this air supply system, affects widely the reaction front stability during the biomass gasification process.

The velocity distribution in the secondary holes ring is more uniform as the number of air inlets increases around the secondary air chamber, for this reason, it was important to look for a balanced design to allow a good distribution of the air in that zone, encompassing low manufacturing cost and the low flow measuring equipment costs. The M2 configuration fulfills all of these characteristics. Therefore, we state that the operation with axial fans, in the final cookstove design, allows obtaining a good standard deviation of air velocity through the grate holes and through secondary air ring holes (±0.13 m/s, and ±0.45 m/s, respectively), which entails a better cookstove performance. A better performance refers to higher thermal energy efficiency (low biomass consumption) and lower emissions.

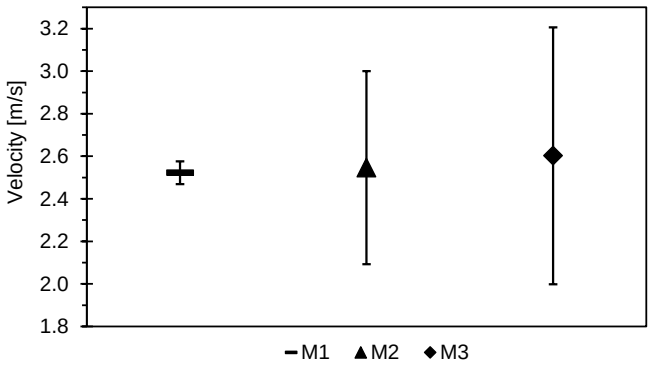

Fig. 13. Standard deviation of velocity through the secondary air holes for the producer gas combustion process.

The diameter of the piping which is used to supply the primary air, affects widely the air velocity and its distribution across the grate. As the diameter increases (from 11 mm to 40 mm), the velocity through the grate holes, presented the lowest standard deviation (±0.13 m/s), it leads to an uniform consumption of the fuel, which allows a better mixing between the secondary air and the producer gas.

The design methodology described and applied in this work allows finding trends of the most important parameters such as the biomass consumption rate, which increases 0.79 kg/kW-h according to the cookstove power. It makes possible to use this parameter during several TLUD cookstove designs making the sizing process widely efficient. On the other hand, in future works, the stove will be constructed, characterized, and contrasted, with model results.

Acknowledgments

The authors acknowledge the Universidad de Antioquia through the project Gimel group “Sostenibilidad 2016-2017”

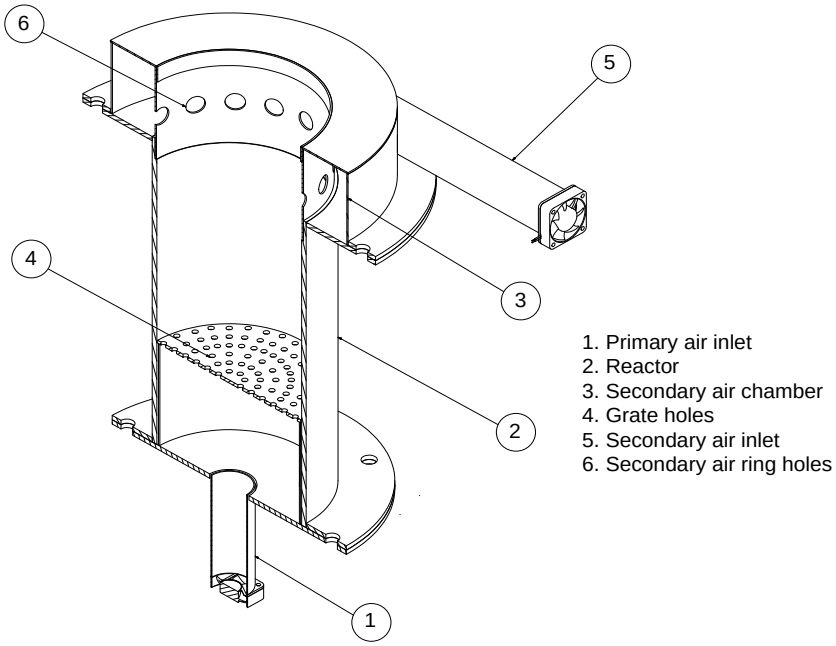

Fig. 14. Isometric of the final TLUD cookstove design.

Nomenclature

$\dot{m}_{bms}$	Biomass consumption rate $[kg\ s^{-1}]$	Y_i	Molar fraction of i $[-]$
E	Cookstove efficiency [%]	n_i	Moles of i $[mol]$
Q	Power $[kW]$	n_T	Total moles $[mol]$
LHV	Low heating value $[kJ\ kg^{-1}]$	$(A/F)stq, g$	Stoichiometric air-producer gas ratio $[-]$
D	Reactor diameter $[m]$	$\dot{m}_{ac}$	Secondary air flow $[kg\ s^{-1}]$
$\dot{m}'_{bms}$	Specific biomass consumption rate$[kg\ m^{-2}\ s^{-1}]$	$\dot{m}_g$	Producer gas flow $[kg\ s^{-1}]$
h	Bed height $[m]$	$\dot{V}_{g,norm}$	Producer gas volumetric flow under normal conditions $[m^3\ s^{-1}]$
den_{bms}	Bulk density $[kg\ m^{-3}]$	$\dot{V}_{air,std}$	Air volumetric flow under standard conditions $[m^3\ s^{-1}]$
t	Biomass consumption time $[s]$	$den_{N_{2,std}}$	Nitrogen density under standard conditions $[kg\ m^{-3}]$
w	Aeration factor $[-]$	$den_{N_{2,norm}}$	Nitrogen density under normal conditions $[kg\ m^{-3}]$
$(A/F)real$	Real air-fuel ratio $[-]$	$Y_{N_{2,air}}$	Molar fraction of nitrogen in the air $[-]$
$(A/F)stq$	Stoichiometric air-fuel ratio $[-]$	$Y_{N_{2,g}}$	Molar fraction of nitrogen in the producer gas
a	Moles of air $[kg\ kmol^{-1}]$	$den_{g,norm}$	Producer gas density under normal conditions $[kg\ m^{-3}]$
M_a	Molecular weight of air $[kg\ kmol^{-1}]$	N	Number of holes
M_{bms}	Molecular weight of biomass $[kg\ kmol^{-1}]$.	P	Perimeter of cylinder where the secondary holes ring is placed $[m]$
$\dot{V}_a$	Gasification volumetric air flow $[m^3\ s^{-1}]$	d_1	Secondary holes diameter $[m]$
$(A/F)stq$	Stoichiometric air-flow ratio $[-]$	b	Separation among secondary holes $[m]$
den_a	Air density $[kg\ m^{-3}]$	v	Velocity of air through secondary holes $[m\ s^{-1}]$
i	Specie $[-]$	$\dot{V}_{ac}$	Combustion air volumetric flow $[m^3\ s^{-1}]$

References

[1] A. Molino, S. Chianese, and D. Musmarra, "Biomass gasification technology: The state of the art overview," *Journal of Energy Chemistry*, vol. 25, pp. 10–25, 2016.

[2] M. A. Gonzalez-salazar, M. Morini, M. Pinelli, P. Ruggero, M. Venturini, M. Finkenrath, and W. Poganietz, "Methodology for estimating biomass energy potential and its application to Colombia," *Applied Energy*, vol. 136, pp. 781–796, 2014.

[3] C. A. Ochieng, C. Tonne, and S. Vardoulakis, "A comparison of fuel use between a low cost , improved wood stove and traditional three-stone stove in rural Kenya," *Biomass and Bioenergy*, vol. 58, pp. 258–266, 2013.

[4] R. Mal, R. Prasad, and V. K. Vijay, "Design and testing of thermoelectric generator embedded clean forced draft biomass cookstove," 2015 IEEE 15th International Conference on Environment and Electrical Engineering, EEEIC 2015 - Conference Proceedings, pp. 95–100, 2015.

[5] T. Kirch, P. R. Medwell, and C. H. Birzer, "Natural draft and forced primary air combustion properties of a top-lit up-draft research furnace," *Biomass and Bioenergy*, vol. 91, pp. 108–115, 2016.

[6] M. P. Kshirsagar and V. R. Kalamkar, "A comprehensive review on biomass cookstoves and a systematic approach for modern cookstove design," *Renewable and Sustainable Energy Reviews*, vol. 30, pp. 580–603, 2014.

[7] P. Lloyd, H. Annegarn, and C. Pemberton-Pigott, "Towards a standard for clean solid-fuelled cookstoves," 2015 International Conference on the Domestic Use of Energy (DUE), pp. 13–17, 2015.

[8] WHO, "Global Health Risks: Mortality and burden of disease attributable to selected major risks," *Bulletin of the World Health Organization*, vol. 87, pp. 646–646, 2009.

[9] M. Obaidullah and S. Bram, "A review on particle emissions from small scale biomass combustion," International Journal of renewable energy research, vol. 2, no. 1, pp. 147–159, 2012.

[10] J. M. Santos Calderon, G. Vallejo Lopez, V. S. Pablo, F. J. Gómez Montes, and R. Suarez Castaño, *Estufas eficientes para cocción con leña*. 2015.

[11] S. T. Rinne, E. J. Rodas, B. S. Bender, M. L. Rinne, J. M. Simpson, R. Galer-unti, and L. T. Glickman, "Relationship of pulmonary function among women and children to indoor air pollution from biomass use in rural Ecuador," *Respiratory Medicine*, vol. i, pp. 1208–1215, 2006.

[12] J. Soto-Moreno and F. Ballester-Díez, "Contaminación del aire de interiores en hogares en situación de pobreza extrema en Colombia," *Rev. salud pública*, vol. 15, pp. 80–89, 2013.

[13] K. S. Thacker, C. A. Mattson, and M. Barger, "A Global Review of End User Needs : Establishing the Need for Adaptable Cookstoves," Proceedings of the IEEE 2014 Global Humanitarian Technology Conference, 2014.

[14] J. Tryner, J. W. Tillotson, M. E. Baumgardner, J. T. Mohr, M. W. DeFoort, and A. J. Marchese, "The Effects of Air Flow Rates, Secondary Air Inlet Geometry, Fuel Type, and Operating Mode on the Performance of Gasifier Cookstoves," *Environmental Science & Technology*, pp. 9754–9763, 2016.

[15] S. Varunkumar, N. K. S. Rajan, and H. S. Mukunda, "Experimental and computational studies on a gasifier based stove," *Energy Conversion and Management*, vol. 53, pp. 135–141, 2012.

[16] T. B. Reed, E. Anselmo, and K. Kircher, "Testing & Modeling the Wood-Gas Turbo Stove," *Progress in Thermochemical Biomass Conversion*, pp. 693–704, 2008.

[17] T. Kirch, C. H. Birzer, P. R. Medwell, and L. Holden, "The role of primary and secondary air on wood combustion in cookstoves," *International Journal of Sustainable Energy*, vol. 6451, pp. 1–10, 2016.

[18] D. Still, S. Bentson, and H. Li, "Results of Laboratory Testing of 15 Cookstove Designs in Accordance with the ISO/IWA Tiers of Performance," *EcoHealth*, vol. 12, pp. 12–24, 2015.

[19] S. Varunkumar, "Packed bed gasification-combustion in biomass based domestic stoves and combustion systems," Indian Institute of Science, 2012.

[20] M. Njenga, M. Iiyama, R. Jamnadass, H. Helander, L. Larsson, J. de Leeuw, H. Neufeldt, K. Röing de Nowina, and C. Sundberg, "Gasifier as a cleaner cooking system in rural Kenya," *Journal of Cleaner Production*, vol. 121, pp. 208–217, 2015.

[21] R. Karmvir Singh, "Design modifications and comparative study of different biomass cookstoves," 2013.

[22] C. Roth, "Micro-Gasification: Cooking with gas from biomass." [Online]. Available: http://lists.bioenergylists.org/pipermail/estufas_lists.bioenergylists.org/attachments/20140305/9f00378b/attachment-0006.pdf. [Accessed: 20-Sep-2016].

[23] S. Mohapatra and K. Gadgil, "Biomass: The Ultimate Source of Bio Energy," *International Journal of Renewable Energy Research*, vol. 3, pp. 2–5, 2013.

[24] N. G. Johnson and K. M. Bryden, "The impact of cookstove adoption and replacement on fuelwood savings," Proceedings - 2012 IEEE Global Humanitarian Technology Conference, GHTC 2012, pp. 387–391, 2012.

[25] J. M. S. Calderón, G. V. López, P. V. Samper, F. J. G. Montes, and R. S. Castaño, "Estufas eficientes para cocción con leña," *Minambiente*, 2015.

[26] U. N. Fundation, "Global Alliance for Clean Cookstoves." [Online]. Available: http://cleancookstoves.org/. [Accessed: 22-Mar-2017].

[27] W. Bank, "Scaling-Up Access to Clean Cooking Technologies and Fuels in Sub-Saharan Africa," pp. 1–10, 2012.

[28] EnDev, "Energising Development." [Online]. Available: http://endev.info/content/Main_Page. [Accessed: 22-Mar-2017].

[29] T. Kirch, P. R. Medwell, and C. H. Birzer, "Natural draft and forced primary air combustion properties of a top-lit up-draft research furnace," *Biomass and Bioenergy*, vol. 91, pp. 108–115, 2016.

[30] V. Issue and T. S. Saloop, "A Study on the Biomass Cook Stoves Used in Kerala and to Develop a Theoretical Design of TLUD Natural Draft Gasifier Stove as an Option for Kerala's Cooking Culture," *International Journal of Innovate Research and Development*, vol. 5, pp. 414–419, 2016.

[31] J. Porteiro, D. Patiño, J. Collazo, E. Granada, J. Moran, and J. L. Miguez, "Experimental analysis of the ignition front propagation of several biomass fuels in a fixed-bed combustor," *Fuel*, vol. 89, pp. 26–35, 2010.

[32] A. Melgar, J. F. Pérez, H. Laget, and A. Horillo, "Thermochemical equilibrium modelling of a gasifying process," *Energy Conversion and Management*, vol. 48, pp. 59–67, 2007.

[33] J. F. Pérez, A. Melgar, and A. Horrillo, "Thermodynamic methodology to support the selection of feedstocks for decentralised downdraft gasification power plants," *International Journal of Sustainable Energy*, vol. 6451, pp. 1–19, 2016.

[34] L. E. G. Fernandez, "Obtención de gas combustible a partir de la gasificación de biomasa en un reactor de lecho fijo," 2011.

[35] M. M. Smith, J. M.; Van Ness, H. C.; Abbott, *Introducción a la Termodinámica en Ingeniería Química*, 5ta Edició. Mc Graw Hill, 1997.

[36] Y. A. Lenis, J. F. Pérez, and A. Melgar, "Fixed bed gasification of Jacaranda Copaia wood: Effect of packing factor and oxygen enriched air," *Industrial Crops and Products*, vol. 84, pp. 166–175, 2016.

[37] M. Michael J and C. Howard N, *Fundamentals of Engineering Thermodynamics*, Fith editi. Wiley, 2001.

[38] H. S. Mukunda, S. Dasappa, P. J. Paul, N. K. S. Rajan, M. Yagnaraman, D. R. Kumar, and M. Deogaonkar, "Gasifier stoves – science , technology and field outreach," *Articles, General*, vol. 98, 2010.

[39] Y. A. Cengel and M. A. Boles, *Termodinámica*, Séptima Ed. Mc Graw Hill, 2011.

[40] "Perfiles y Vigas." [Online]. Available:

http://www.perfilesyvigas.com/. [Accessed: 25-Oct-2016].

[41] J. Collazo, J. Porteiro, D. Patiño, and E. Granada, "Numerical modeling of the combustion of densified wood under fixed-bed conditions," *Fuel*, vol. 93, pp. 149–159, 2012.

[42] J. F. Pérez, A. Melgar, and P. N. Benjumea, "Effect of operating and design parameters on the gasification/combustion process of waste biomass in fixed bed downdraft reactors: An experimental study," *Fuel*, vol. 96, pp. 487–496, 2012.